NeuroImage 283 (2023) 120435

Contents lists available at ScienceDirect

NeuroImage

journal homepage: www.elsevier.com/locate/ynimg

Human brain mapping using co-registered fUS, fMRI and ESM during awake brain surgeries: A proof-of-concept study

S. Soloukey [a,b], E. Collée [b], L. Verhoef [a], D.D. Satoer [b], C.M.F. Dirven [b], E.M. Bos [b], J.W. Schouten [b], B.S. Generowicz [a], F. Mastik [a], C.I. De Zeeuw [a,c], S.K.E. Koekkoek [a], A.J.P.E. Vincent [b], M. Smits [d], P. Kruizinga [a,*]

[a] Department of Neuroscience, Erasmus MC, Wytemaweg 80 3015 CN, Rotterdam 3015 CN, the Netherlands
[b] Department of Neurosurgery, Erasmus MC, Rotterdam 3015 CN, the Netherlands
[c] Netherlands Institute for Neuroscience, Royal Dutch Academy for Arts and Sciences, Amsterdam 1105 BA, the Netherlands
[d] Department of Radiology and Nuclear Medicine, Erasmus MC, Rotterdam 3015 CN, the Netherlands

ARTICLE INFO

Keywords:
Functional Ultrasound
Functional MRI
Electrocortical stimulation mapping
Awake craniotomy
Functional imaging
Neurovascular coupling

ABSTRACT

Accurate, depth-resolved functional imaging is key in both understanding and treatment of the human brain. A new sonography-based imaging technique named functional Ultrasound (fUS) uniquely combines high sensitivity with submillimeter-subsecond spatiotemporal resolution available in large fields-of-view. In this proof-of-concept study we show that: (A) fUS reveals the same eloquent regions as found by fMRI while concomitantly visualizing *in-vivo* microvascular morphology underlying these functional hemodynamics and (B) fUS-based functional maps are confirmed by Electrocortical Stimulation Mapping (ESM), the current gold-standard in awake neurosurgical practice. This unique cross-modality experiment was performed using motor, visual and language-related functional tasks in patients undergoing awake brain tumor resection. The current work serves as an important milestone towards further maturity of fUS as well as a novel avenue to increase our understanding of hemodynamics-based functional brain imaging.

1. Introduction

Functional imaging of the human brain is of vast importance for both clinical diagnostics and neuroscientific understanding. The majority of currently available functional brain imaging techniques struggle to combine favorable technical features such as high spatiotemporal resolution with deep penetration or high sensitivity, often providing one at the cost of the other (Deffieux et al., 2018). Blood-Oxygenation-Level-Dependent (BOLD) imaging - the most commonly used functional magnetic resonance imaging (fMRI) technique – is a clinical and neuroscientific tool for non-invasive functional brain mapping (Hacker et al., 2019; Vlieger et al., 2004). In the clinical context, BOLD-fMRI is often used as a pre-operative technique to aid in neurosurgical planning (Stopa et al., 2020) and involves conventional 1.5–3.0T MRI-systems, providing millimeter-second spatiotemporal resolution (Hacker et al., 2019; Stopa et al., 2020; Vlieger et al., 2004).

Electrocortical Stimulation Mapping (ESM), also known as Direct Electrical Stimulation (DES), is considered to be one of the most direct tools for functional interrogation of the brain (Ritaccio et al., 2018). During awake craniotomy surgery for tumor removal, ESM is used by neurosurgeons to interact with the exposed human brain by stimulating regions of interest of the cortex. Based on the patient's behavioral response, ESM helps create functional maps around the tumor which help guide intra-operative decision-making during tumor removal. To this day, ESM remains a limited, non-standardized technique with low spatial resolution (~1 cm), limited penetration depths (< 1 cm) and with considerable risks of false positives and even side-effects such as seizure elicitation (Borchers et al., 2011; Ritaccio et al., 2018).

Functional Ultrasound (fUS) is a new functional neuroimaging technique (Deffieux et al., 2018) introduced over a decade ago (Macé

Abbreviations: 2PM, two-photon microscopy; BF, beamformed frames; BOLD, blood-oxygenation-level-dependent; CBV, cerebral blood volume; CDI, color Doppler image; CT, computed tomography; DES, direct electrical stimulation; ESM, electrocortical stimulation mapping; fMRI, functional MRI; FSPGR, fast spoiled gradient recalled echo; fUS, functional Ultrasound; HGG, high grade glioma; LGG, low grade glioma; MRI, magnetic resonance imaging; NVC, neurovascular coupling; PDI, power Doppler image; ROI, region of interest.

* Corresponding author.
E-mail address: p.kruizinga@erasmusmc.nl (P. Kruizinga).

https://doi.org/10.1016/j.neuroimage.2023.120435
Received 27 July 2023; Received in revised form 15 October 2023; Accepted 29 October 2023
Available online 30 October 2023

et al., 2011), with current applications in rodents (Errico et al., 2016; Gesnik et al., 2017; Osmanski et al., 2014; Rabut et al., 2019; Urban et al., 2015), pigeons (Rau et al., 2018), non-human primates (Dizeux et al., 2019; Norman et al., 2021), neonates (Baranger et al., 2021; Demene et al., 2017) and adult humans (Imbault et al., 2017; Soloukey et al., 2020). fUS is based on high-sensitivity high-frame-rate Doppler ultrasound imaging of microvascular haemodynamics, including changes in cerebral blood flow (CBF), cerebral blood volume (CBV) and vascular tonus (Deffieux et al., 2018; Mace et al., 2013; Macé et al., 2011; Nunez-Elizalde et al., 2022; Soloukey et al., 2020). By virtue of neurovascular coupling (NVC), these hemodynamics serve as an indirect measure of neuronal activity (Deffieux et al., 2018; Iadecola, 2017; Soloukey et al., 2020). In contrast to many other conventional functional brain imaging modalities such as fMRI, fUS combines its high sensitivity (Macé et al., 2011) with submillimeter-subsecond spatiotemporal resolution and large fields of view without the need for contrast agents (Deffieux et al., 2018). In two previous studies (Imbault et al., 2017; Soloukey et al., 2020), fUS was able to delineate deep (> 5 cm) functional brain areas in awake patients performing language and motor-related tasks during tumor resection. With the number of fUS-applications expanding rapidly in the last decade, fUS might quickly become a new neuro-imaging modality of relevance.

In theory, fUS, ESM and fMRI would be sensitive to different components of the same mechanism of NVC, where spontaneous or stimulus-evoked neuronal activity is thought to cause a complex interplay of changes in (oxidative) metabolism, CBV, CBF and vascular tonus. Different vascular compartments (i.e. arteries, arterioles, capillaries, venules and veins), are thought to contribute differently in this process (Martin, 2014; Uludağ and Blinder, 2018). However, many questions on the underlying mechanisms responsible for NVC in health and disease remain unanswered, many of which would benefit from a multi-modal approach in the same human subject. However, to date, there is no record of a direct, in-human comparison between fUS-acquired, hemodynamics-based functional maps and its already widely established counterparts of BOLD-fMRI or ESM.

Here we report the first in-human fMRI- and ESM-confirmed fUS-images of human brain function acquired during motor, language and visual tasks in three patients undergoing neurosurgical intervention. We demonstrate how fUS-acquired functional areas overlap with areas found with pre-operative fMRI as well as intra-operative ESM. We also show the additional abilities of fUS to concomitantly visualize *in-vivo* microvascular morphology at high penetrative depths, currently missing in other modalities. In order to achieve this multi-modal comparison, we designed unique, intra-operative experiments on the exposed human brain involving an intricate technical ecosystem to achieve real-time co-registered fUS-, ESM- and fMRI-mapping in the same human subject. The details of this technical ecosystem will also be discussed in this paper. Finally, we discuss the potential of comparing fMRI and fUS for increasing our understanding of hemodynamics-based functional imaging and neurovascular coupling (NVC) in general.

2. Materials and methods

2.1. Subject inclusion and ethics statement

The data presented in this paper involves measurements in three patients with a brain tumor planned for awake surgical resection. Patients were recruited from the Department of Neurosurgery of Erasmus MC in Rotterdam. Prior to inclusion, written informed consent was obtained in line with the National Medical-Ethical Regulations (MEC-2018–037, NL64082.078.17).

2.2. Study procedure and functional paradigms

Patients underwent a pre-operative fMRI-scan of max. 30 min., in which a total of max. 4 functional tasks were presented. Functional tasks were selected based on patient's pre-operative, language/cognitive level of functioning (as assessed by a clinical linguist (*KEC/DDS*)) and anatomical location of the tumor. The functional task paradigm for the fMRI-measurements consisted of an alternating 30 s ON, 30 s OFF-pattern, as visualized in Supplementary Table 1. This functional task pattern has been tried-and-tested for years in the clinical context of pre-operative functional mapping in our academic center.

Intra-operatively, patients first underwent a conventional clinical Electrocortical Stimulation Mapping (ESM)-procedure, where direct bipolar electrical stimulation of the brain surface was used to determine presence of so-called eloquent brain areas involved in functional tasks such as speech (Fig. 1A–E). Based on the functional response during ESM, a selection of intra-operative functional tasks was presented to the patient using a tablet while acquiring fUS-data (Fig. 1C), with a total imaging duration of max. 20 min.

Intra-operative fUS-tasks were similar to fMRI-tasks in design, but with a different functional task-pattern. For the fUS-tasks we opted for ON-blocks chosen randomly between 4 and 16 s, followed by an off-period chosen randomly between 4 and 15 s to minimize the predictability of the stimulus for the participant and improve fUS-signal decoupling from periodic physiological signals (see Supplementary Table 1). These short ON- and OFF-times were not suitable for the clinical 3T fMRI-scanner that was available to us, as the pulse repetition frequency would be too long to capture enough datapoints in our shorter ON-blocks (see also Section 2.3.1). Therefore, we decided to adhere to the clinical functional paradigm for the fMRI acquisitions as described above. The other way around, the clinical fMRI-paradigm was not suitable for the fUS-acquisitions, as the longer ON-tasks proved to be too tiring for the intra-operative setting. Only in patient #3 did we manage to do one longer fUS-acquisition, as the visual task was experienced as less strenuous (see Supplementary Table 1).

2.3. Data acquisition

2.3.1. Functional MRI (fMRI)

MR Imaging was performed pre-operatively using a 3.0T-scanner with an 8-channel head coil (Discovery MR750, GE Healthcare, Milwaukee, WI, US). Whole brain functional MR images were obtained with a single shot T2* weighted EPI sequence sensitive to BOLD contrast with the following parameters: repetition time (TR) = 3000 ms, sampling frequency (Fs) = 0.33 Hz, echo time (TE) = 30 ms, flip angle = 90°, acquisition matrix = 96×64, field of view (FOV) = 240×180 mm^2. We acquired 54 slices with a slice thickness of 2.2 mm and 0.3 mm gap, resulting in an fMRI-voxel size of 2.6 mm x 2.8 mm x 2.5 mm. Functional data acquisition started with 5 dummy scans, which were discarded from further analysis. Patients received instructions and practiced the fMRI task together with a researcher (*KEC*) 15 min prior to MRI scanning. During scanning, stimuli were visually presented outside the scanner onto an MRI compatible monitor that was visible with a mirror mounted on the head coil. Patients wore MRI-compatible glasses for correction of vision if needed. Additionally, a high-resolution 3D T1-weighted inversion recovery fast spin gradient recalled echo (IR FSPGR) structural MRI was acquired in the axial plane with the following parameters: TR = 7.93 ms, TE = 3.07 ms, inversion time = 450 ms, flip angle = 12°, acquisition matrix = 240×240, FOV = 240×240 mm^2. 176 contiguous slices were acquired with a slice thickness of 1 mm, resulting in an MRI-voxel size of 1 mm x 1 mm x 1 mm. Prior to the surgical procedure, the pre-operative fMRI-based functional maps were outlined manually on the navigational CT/MRI-volumes using the Brainlab '*Cranial Planning*' module (Fig. 1F).

2.3.2. Electrocortical stimulation mapping (ESM)

During the surgical procedure, the conventional clinical workflow was adhered as much as possible. The patient was prepped and positioned for surgery in the Mayfield skull clamp and after the cranio- and durotomy, the conventional ESM-procedure was performed.

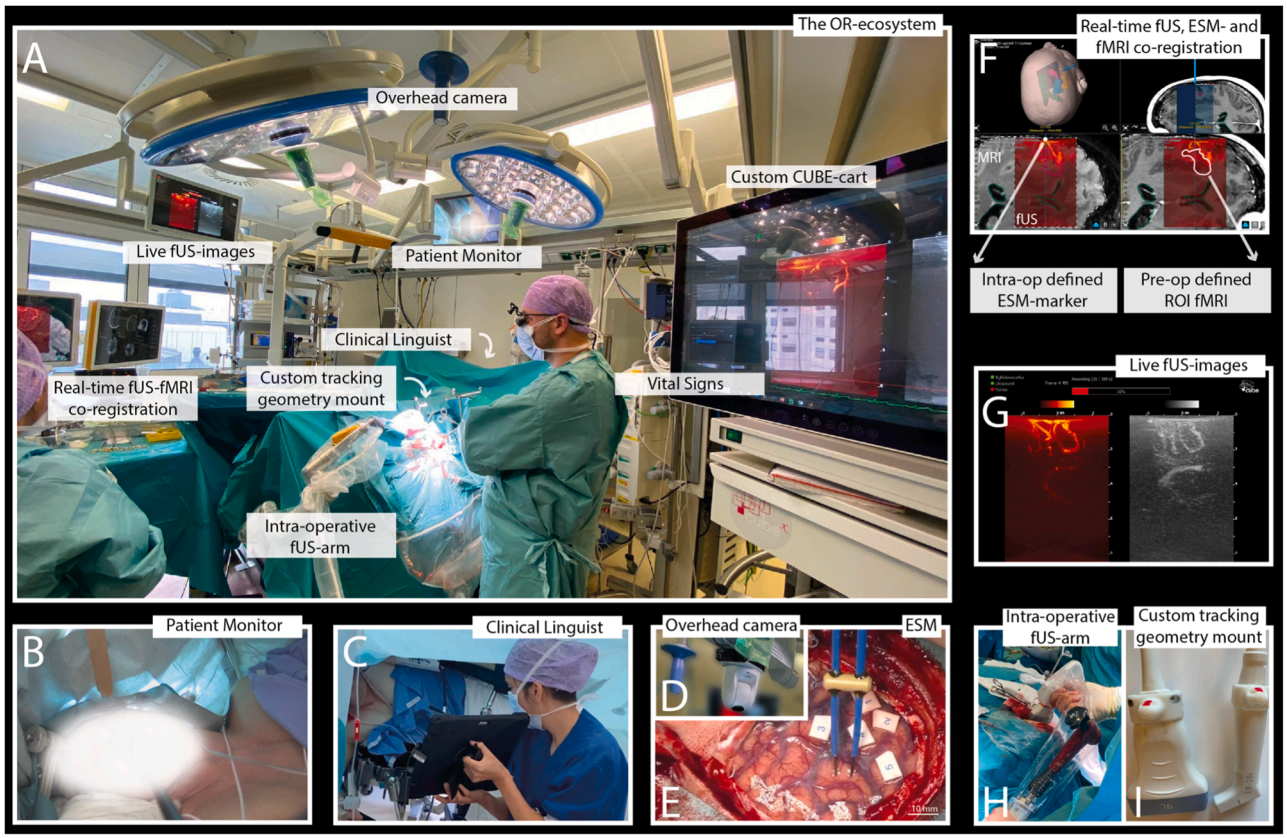

Fig. 1. Overview of the ecosystem necessary to facilitate real-time fUS-fMRI co-registration in the intra-operative context. (**A**) Overview of the OR during a fUS-acquisition. As becomes clear from the picture, our fUS-data is fully integrated into the conventional clinical workflow. (**B**) During the full surgical procedure, including our fUS-acquisitions, the awake patient is monitored (video and audio), to use as a reference for offline functional analyses. (**C**) During fUS-acquisitions, the clinical linguist presents functional tasks to the patient using a hand-held tablet. (**D**) An overhead camera records the surgical field as the surgeon performs ESM and removes the tumor. These recordings are synchronized to the audiovisual recordings of the patient, allowing for further offline analyses of functional behavior. (**E**) Surgeon's view of the craniotomy during the ESM-procedure. The bipolar electrode (*blue*) is used to interrogate the brain tissue. Hotspots which were involved in production or disruption of functionality were marked using numbered cut-outs, which were later manually stored in the Brainlab environment using the navigation pointer. **F**) Screenshot of the intra-operative Brainlab-screen displaying our PDIs co-registered to the pre-operative MRI and fMRI ROIs as well as the stored ESM-hotspots in real-time. (**G**) Through integration of our experimental cart in the OR-system, our live PDIs were displayed in real-time on the OR-screens, as well as in the Brainlab-system as MR/CT co-registered overlays. (**H**) To minimize motion-artefacts during our functional recordings, the probe was stabilized over an ROI using a custom surgical arm, modified in-house. (**I**) To co-register our PDIs in real-time in the OR, our transducers were made trackable by Brainlab neuronavigation software by attaching the conventional optical tracking geometry to the transducer casing using custom-made 3D-printed attachments.
fUS = functional Ultrasound, ESM = Electrocortical Stimulation Mapping, PDI = Power Doppler Image, ESM = Electrocortical Stimulation Mapping, CT = Computed Tomography, (f)MRI = (functional) Magnetic Resonance Imaging, ROI = Region of Interest.

Using a bipolar electrode (Yasargil Non-Stick Mirror Finish Insulated Bipolar Forceps, bayonet) connected to a cortical stimulation unit (Grass Technologies, Astro-Med, Inc.), square-wave pulses were delivered to induce depolarization of relevant cortices. The bipolar electrode was customized in house by fixating the distance between the forceps-tips at 5 mm (see Fig. 1E), with a tip size of 1.0 mm. According to standard protocol, the intensity of the working current was increased from 6 to maximum 12 mA (60 Hz, 1 ms), depending on whether a functional effect was evoked. A functional effect could be positive (i.e. production of a movement or sensation) or negative (i.e. disruption of behavior such as speech or movement). Any unusual production or disruption of behavior was monitored and shared with the OR-team by the clinical linguist (*KEC/DDS*) guiding the patient's surgical procedure. In some cases, no functional effect was found, even at maximum current intensity. Eloquent areas, if found during ESM, were labeled with numbers (see Fig. 1E) and the functional effect corresponding each hotspot would be logged for future reference. Once the ESM-procedure was complete, the coordinates of each of the numbered labels would be stored and displayed intra-operatively using the conventional navigation pointer, as part of Brainlab '*Cranial Navigation*' module (Fig. 1F).

2.3.3. *Functional Ultrasound (fUS)*

fUS-acquisitions were performed using an experimental research system (Vantage-256, Verasonics) interfaced with the L8–18I-D linear array hockey stick transducer (GE, 7.8 MHz) or 9L-D linear array transducer (GE, 5.3 MHz). For all scans we acquired continuous angled plane wave acquisition (10–12 angles equally spaced between −12 and 12°) with a PRF ranging from 667 to 800 Hz depending on the imaging depth and transducer. The average ensemble size (number of frames used to compute one Power Doppler Image (PDI)) was set at 200 frames from which the live PDIs were computed, providing a live Doppler FR ranging between 3 and 4 Hz (Fig. 1G). Patient's vital signs (EKG, arterial blood pressure) were recorded using a National Instruments' *Compact-DAQ* module (NI 9250) and stored for post-processing purposes. The PDIs as well as the raw, angle compounded beamformed frames (BFs) were stored to a fast PCIe SSD hard disk for offline processing purposes.

Intra-operatively, the transducer was placed over those functional Regions of Interest (ROIs) that were both ESM-defined and overlapped with fMRI-functional maps based on real-time intra-operative fUS-fMRI co-registration (Fig. 1F). In all cases, the transducer was stabilized over the ROI using a customized intra-operative surgical arm (*Trimano, Gettinge*) with transducer-holder during functional acquisitions (Fig. 1H).

To co-register our PDIs to the ESM- and fMRI-hotspots in real-time in the OR, our transducers were made trackable by Brainlab neuronavigation software by attaching the conventional optical tracking geometry to the transducer casing using custom-made 3D-printed attachments (Fig. 1I). Using the 'IGTLink' research interface, we could store real-time tracking data for offline post-processing. The co-registration and tracking system was thought to have millimeter-range precision. Prior to durotomy, a hand-held 3D-volume of the tumor was obtained by acquiring 2D-images during a 60 s sweeping motion along a continuous trajectory.

2.4. Post-processing

2.4.1. Post-operative brain shift correction

Any remaining brain-shift related fUS-fMRI mismatches were corrected offline using 3D Slicer (Fedorov et al., 2012). A rigid linear transform was found for each individual dataset by manually re-aligning the ultrasound Bmode to the structural 3D MRI-volume. The accuracy of the re-alignment was visually confirmed using morphological details in the PDI (e.g. comparing the position of sulcal arteries in the PDI with the position of sulci in the structural MRI).

2.4.2. Functional MRI (fMRI)

fMRI-analysis was performed offline using Statistical Parametric Mapping (SPM8, Functional Imaging Laboratory, UCL, UK) implemented in Matlab (vR2015b). For each patient, we first spatially realigned all fMRI-images and co-registered these images to the individual's T1-weighted image, using a rigid body transformation as implemented within SPM8. We used the intra-operative positional information to compute the arbitrary 2D-fMRI slice corresponding to the fUS-slice.

2.4.3. Electrocortical stimulation mapping (ESM)

The coordinates of each of the ESM hotspots were extracted from the stored data in the Brainlab software and loaded into Matlab (vR2021b) to build an ESM-volume. First, each ESM-hotspot was used as the center of a 3D-gaussian kernel with a sigma corresponding to 5 mm, in line with literature on bipolar electrical stimulation of the human brain (Nathan et al., 1993). Next, the ESM-volume was masked for the brain's surface. To display the 3D ESM-hotspots on the brain's surface we made us of ParaView software (2022 Kitware, Inc.). We used the intra-operative positional information to compute the arbitrary 2D-ESM slice corresponding to the fUS-slice.

2.4.4. Functional Ultrasound (fUS)

PDIs were computed using an SVD clutter filter (*cut-off percentage 5 %)* over each ensemble of BFs and mapped onto a 100 μm grid using upsampling in the frequency domain. The ensemble size was adaptively set to match one cardiac cycle based on the acquired EKG-signal, before averaging the power Doppler signal. Offline 3D reconstructions of the linear PDI-scans were made by registering the Power Doppler signals to a 3D volume using the position tracking information obtained through the OpenIGTLink (Tokuda et al., 2009) (http://openigtlink.org/).

2.5. Functional analyses

To ensure comparability, fUS- and fMRI-datasets were then subjected to the same pipeline for functional analyses. To build the functional maps for both fUS- and fMRI-datasets, the Pearson Correlation Coefficient (PCC) 'r' was computed between the temporal pattern of the stimulus signal and either the Power Doppler- (*fUS*) or the BOLD-signal (*fMRI*) for each pixel. Similar to our previous work (Soloukey et al., 2020) we chose the optimal lag between the stimulus signal and fUS data that provided the highest contrast between the background and functional region. Attributed to the slow-time variations in the functional signal the spatial appearance of the functional regions varies slowly with the lag between the fUS data and stimulus. We produced 'overlay-figures', where thresholded (PCC>0.3) functional maps of fUS-only (*yellow)*, fMRI-only (*blue*) and fUS-fMRI overlapping pixels (*red*) were displayed over the mean-PDI or the structural MRI (*both grayscale*).

We used spatial 2D-Gaussian smoothing (*sigma of [4 5] pixels*) of the overlayed functional maps to enhance visibility of functional clusters. Finally, an outline of the 2D-ESM hotspots was drawn over the overlay-figure, to distinguish the 7, 5 and 3 mm zones of activation.

To display the functional signal, all functional pixels in the field of view (i.e. all pixels with a PCC-value >0.3), were averaged into a 'mean functional signal', before normalizing this mean signal by its absolute maximum value. Additionally, the 'background' signal was displayed for comparative purposes with the functional signal. The background-signal consisted of the mean signal of all other pixels deemed as non-functional (PCC-value<0.3).

We also studied the effect of different PCC-thresholds on the overlap between fUS-, ESM- and fMRI functional maps (see Supplementary Fig. 1). Finally, we compared out fMRI-based functional maps using the PCC-methodology described above to fMRI-based functional maps as created using a General Linearized Model (GLM)-approach, a conventional methodology within the fMRI-field (Poldrack et al., 2011) (see Supplementary Fig. 2).

3. Results

3.1. Patient characteristics

The data acquired in a total of $N = 3$ patients is presented in this report. Two of the included patients (*patent 1 and 2*) were suspected to have Low Grade Glioma (LGG), whereas patient 3 was suspected to have a High Grade Glioma (HGG). Other patient characteristics are described in Supplementary Table 2. An overview of all ESM-defined hotspots found intra-operatively for each patient can be found in Supplementary Table 3.

3.2. Language task

Patient 1 (*LGG, left parietal lobe*) performed a paired fUS-fMRI language task focused on sentence completion (see Supplementary Table 1). The probe was positioned over an ESM-confirmed area of the cortical surface involved in language processing known as Wernicke's area (Fig. 2A, B). Prior to the functional recording, a linear ultrasound-scan was made to reconstruct the contextual 3D-vascular morphology (Fig. 2C). Fig. 2D compares the structural PDI and MR-images after fUS-fMRI co-registration. Comparing the fUS- and fMRI-defined functional maps reveals spatial overlap between the two modalities in all three functional clusters that were found (Fig. 2E). Additionally, the ESM-map confirms co-localization of the fUS- and fMR-maps with two of the ESM-hotspots. The average functional signal found with fUS and fMRI is depicted in Fig. 2F.

3.3. Motor task

Patient 1 (*mentioned above*) and Patient 2 (*LGG, left temporal lobe*) both performed a fUS-fMRI lip pouting motor task (see Supplementary Table 1). For patient 1, intra-operative ESM confirmed anatomical localization of the motor cortex of the mouth in the precentral gyrus (Fig. 3A, B). As mentioned previously, prior to the functional recording, a linear ultrasound-scan was made to reconstruct the contextual 3D-vascular morphology (Fig. 3C). Our PDI's showed vessels down to 400 μm in diameter, and showed clear proximity to the tumor tissue (*red dotted line*) (Fig. 3D). Comparison of the fUS- and fMRI-defined functional maps shows complete spatial overlap, with close to no non-overlapping fUS-defined functional areas (Fig. 3E). In contrast, the fMRI-defined functional map seems to span a significantly larger surface area. The ESM-map confirms co-localization of the fUS- and fMRI-map with one of the two ESM-hotspots. The average functional signal found with fUS and fMRI is depicted in Fig. 3F. More details on the

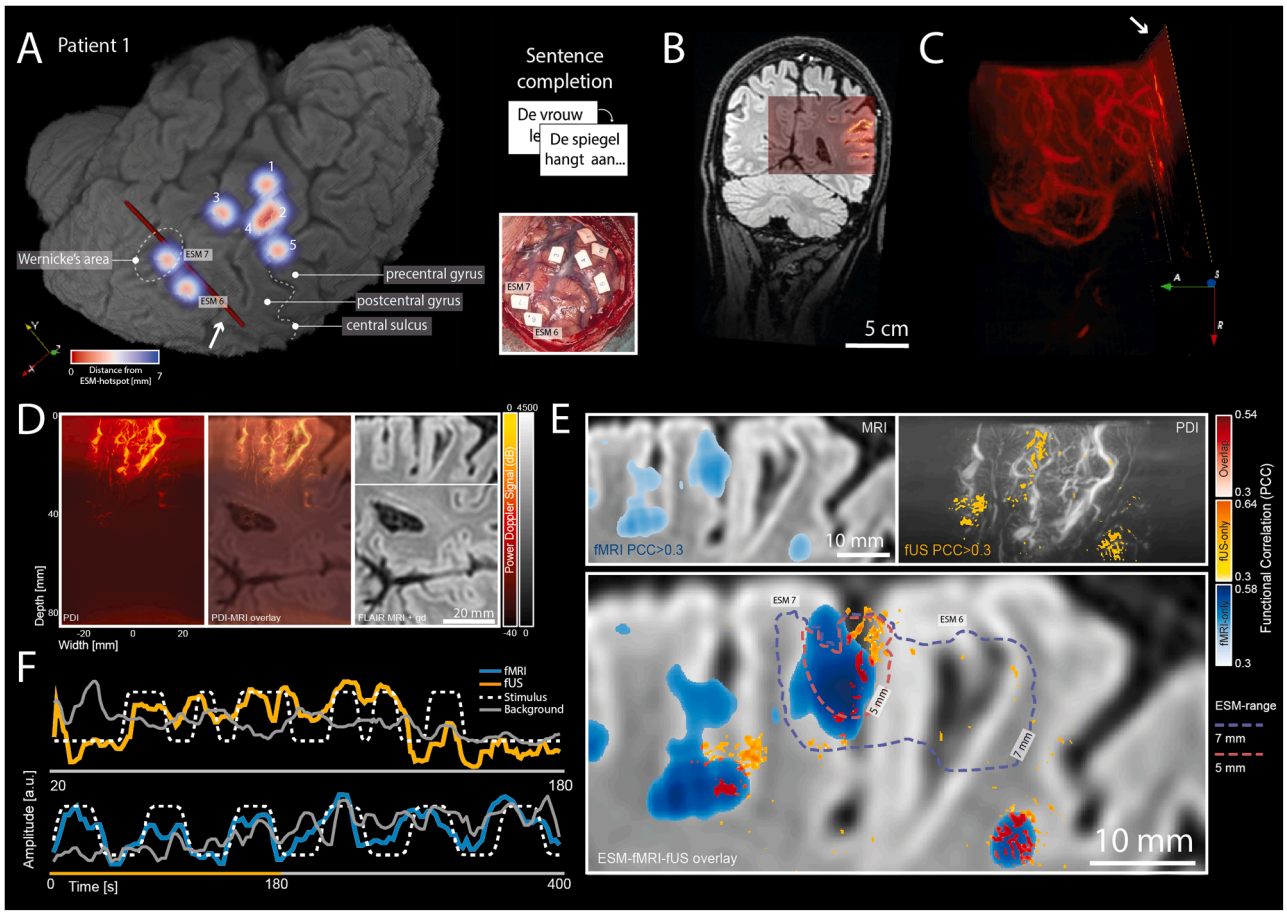

Fig. 2. Paired ESM-, fMRI- and fUS-acquisition in Patient 1: Language Paradigm (sentence completion). (**A**) Patient 1 underwent awake craniotomy surgery for the removal of an LGG in the left parietal lobe. The tumor was localized closely to both the central sulcus (sensorimotor cortex), as well as Wernicke's area (language). Here we show the segmented cerebrum based on the pre-operative 3D T2w-FLAIR MRI after administration of a gadolinium-based contrast agent. Intra-operative ESM was able to identify two stimulation sites (*marker 6–7*) involved in observed speech delays in the patient. These areas were marked as involved in language production (*see also intra-operative picture*), and the probe was placed over this area, co-guided by the pre-operatively defined fMRI-ROIs based on a sentence completion task. The ultrasound plane during the language task is depicted in red here (*white arrow*). (**B**) Depiction of the co-registered MRI-slice corresponding to the 2D-ultrasound plane (*red*) described in (A). (**C**) 3D-vascular volume reconstructed from 2D-PDIs acquired intra-operatively during a sweeping motion over the craniotomy. The position of the functional 2D-PDI plane relative to the 3D-volume is also depicted (*white arrow*). This volume exemplifies the level of microvascular detail which could be visualized intra-operatively using fUS.
(**D**) Side-by-side comparison of the structural 2D-PDI (*left panel)* and corresponding 2D-MR-image (*right panel*), as well as their overlay (*middle panel*). The PDI shows vascular details of healthy cortical vasculature, as well as deeper vascular details toward the ventricle. The white rectangle in the right panel depicts the ROI used for functional analysis. (**E**) Thresholded (PCC>0.3) and smoothed versions of fUS-based (*top right panel*) and fMRI-based (*top left panel*) PCC-maps overlayed over the grayscale PDI in the fUS-based (*left panel*) and structural MRI in the fMRI-based (*right panel*) condition. The bottom panel shows overlap between the fUS- and fMRI-defined functional map in all of the three functional clusters (*red colormap*). Additionally, the image shows the estimated 2D-ESM contour, which overlaps closely with one of the three functional clusters. (**F**) Overview of the functional signal in the fUS-defined functional areas (*yellow line*) and the fMRI-defined functional areas (*blue line*). The stimulus pattern (*white dotted line*) as used for the fUS-recording was significantly shorter and consisted of more randomized ON-durations as compared to the one used pre-operatively for fMRI. The average background signal of all the non-functional (PCC<0.3) pixels within the ROI is depicted in gray. LGG = Low Grade Glioma, (f)MRI = (functional) Magnetic Resonance Imaging, fUS = functional Ultrasound, gd = gadolinium, ESM = Electrocortical Stimulation Mapping, ROI = Region of Interest, PCC = Pearson Correlation Coefficient, PDI = Power Doppler Image.

motor task performed by patient 1 can be found in Supplementary Video 1.

For Patient 2, the positioning of the fUS-probe was also both fMRI- and ESM-guided (Fig. 4A, B). The 3D-reconstruction of the vascular morphology reveals an intricate arborous structure penetrating the tumor's core (*white arrow and red dotted line*) (Fig. 4C–D). Comparison of the fUS-, ESM- and fMRI-defined functional maps shows clear overlap between the three techniques (Fig. 4E), although less clear as compared to the lip pouting task in patient 1. The average functional signal found with each of the techniques is depicted in Fig. 4F.

3.4. Visual task

Patient 3 (*HGG, right parietal lobe*) performed a paired fUS-fMRI visual task involving an 8 Hz flickering checkerboard (see Supplementary Table 1). Intra-operative ESM confirmed anatomical localization of the visual cortex (occipital lobe) due to reported 'flashing' seen by the patient upon stimulation (Fig. 5A, B). The ultrasound probe was positioned over this functional area, co-guided by the pre-operatively defined fMRI-ROIs. The PDI (Fig. 5C–D) shows vascular details of healthy cortical vasculature, including a feather-like horizontal vessel at approximately 2 cm depth (*white arrow*). Comparing the fUS- and fMRI-defined functional maps (Fig. 5E) shows close to complete overlap of the fUS-defined functional map. Additionally, the ESM-map confirms co-localization confirms co-localization of the fUS- and fMRI-map with two of the ESM-hotspots. Interestingly, the fUS-defined functional map seems to clearly follow the architecture of the feather-like vessel, whereas the fMRI-map seems to span a much larger region (Fig. 5F). In

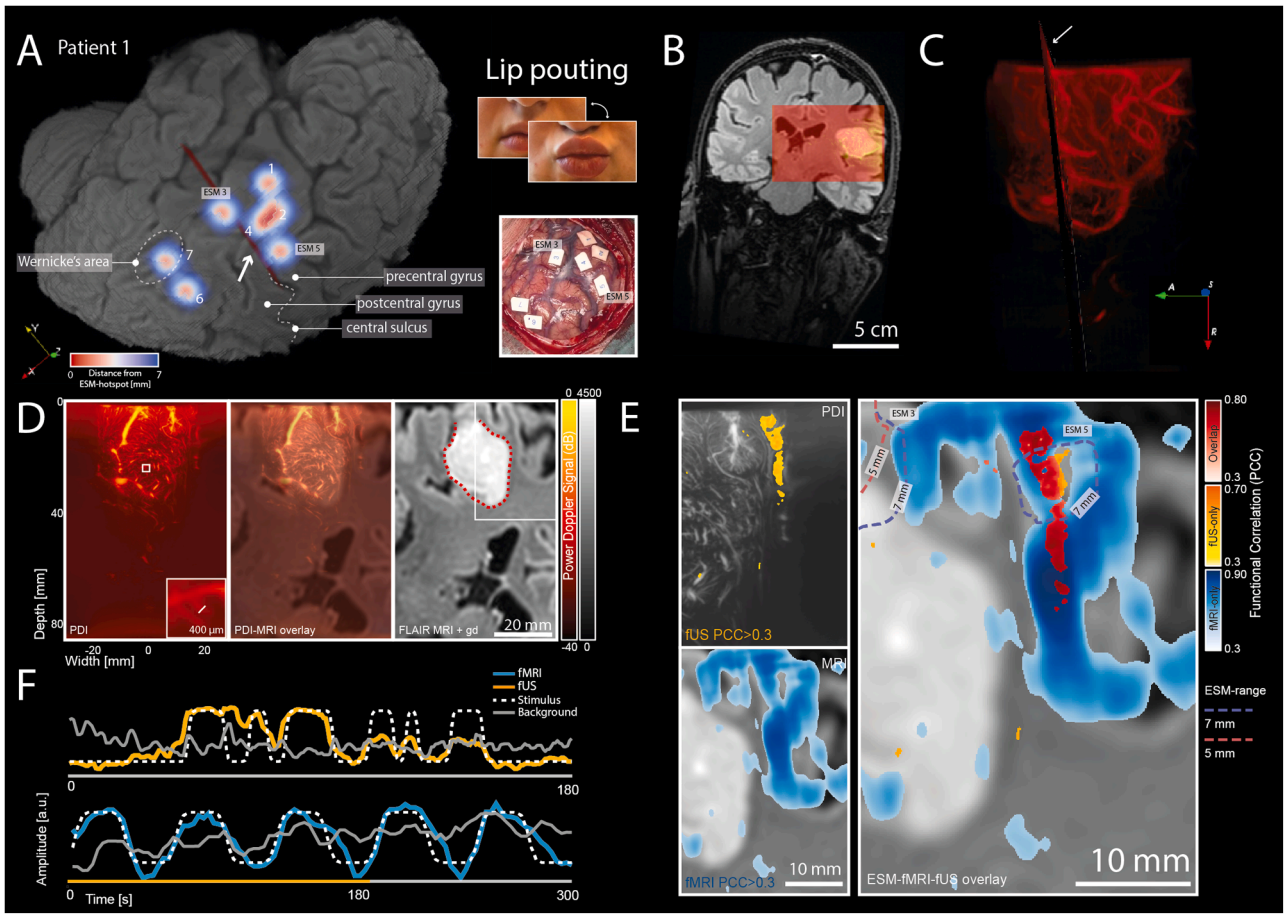

Fig. 3. Paired ESM-, fMRI- and fUS-acquisition in Patient 1: Motor Paradigm (lip pouting), (A) In the same patient (*Patient 1*) as described in Fig. 2, intra-operative ESM was able to identify several additional stimulation sites responsible for twitching of the mouth (*marker 1–5*), confirming the localization of the mouth motor cortex (*precentral gyrus*). The probe was positioned over these areas using the intra-operative arm, co-guided by the pre-operatively defined fMRI-ROIs based on a lip pouting task. The ultrasound plane is again depicted in red here (*white arrow*) and positioned relative to the same 3D-MRI as depicted in Fig. 2. (**B**) Depiction of the co-registered MRI-slice corresponding to the 2D-ultrasound plane (*red*) described in (A). (**C**) 3D-vascular volume reconstructed from 2D-PDIs acquired intra-operatively during a sweeping motion over the craniotomy. Again, the position of the functional 2D-PDI plane relative to the 3D-volume is depicted (*white arrow*). (**D**) Side-by-side comparison of the structural 2D-PDI (*left panel)* and corresponding 2D-MR-image (*right panel*), as well as their overlay (*middle panel*). The overlay confirms the accuracy of the fUS-MRI co-registration. The PDI shows vascular details both inside the tumor (*red dotted contour in right panel*), as well as of the surrounding healthy vasculature at a submillimeter scale and at depths >5 cm. Vessels up to 400 µm could be discerned within the PDI, as depicted in the zoom-in the left panel. The white rectangle in the right panel depicts the ROI used for functional analysis. (**E**) Thresholded (PCC>0.3) and smoothed versions of fUS-based (*left panel*) and fMRI-based (*right panel*) PCC-maps overlayed over the structural MRI or grayscale PDI in the fUS-based (*left panel*) and fMRI-based (*right panel*) condition, as well as with both modalities overlapping (*middle panel*). The middle panel shows a close to complete area of overlap of the fUS-defined functional map within the fMRI-functional map (*red colormap*). In contrast, the fMRI-defined functional area which is non-overlapping (*blue*) is significantly larger. The ESM-map confirms co-localization with one of the two ESM-hotspots. (**F**) Overview of the functional signal in the fUS-defined functional areas (*yellow line*) and the fMRI-defined functional areas (*blue line*). The stimulus pattern (*white dotted line*) as used for the fUS-recording was significantly shorter and consisted of more randomized ON-durations as compared to the one used pre-operatively for fMRI. More details on the motor task performed by patient 1 can be found in **Supplementary Video 1**.

LGG = Low Grade Glioma, (f)MRI = (functional) Magnetic Resonance Imaging, gd = gadolinium, fUS = functional Ultrasound, ESM = Electrocortical Stimulation Mapping, ROI = Region of Interest, PCC = Pearson Correlation Coefficient, PDI = Power Doppler Image.

this case, the functional paradigm as used for the fUS- and fMRI-recording was similar and consisted of alternating 30 s ON- and OFF-periods (Fig. 5G).

4. Discussion

This paper is a first in-human proof-of-concept study confirming spatial overlap between functional maps based on gold standard techniques of ESM and fMRI and functional maps as produced by fUS, a new and highly promising functional brain imaging modality. Like many others in the fUS-community, we believe that we are at the dawn of a more widespread application of fUS as an influential new tool for systems neuroscience and clinical decision-making. In the last decade, numerous advancements have allowed fUS to technically mature from an offline 2D-technique only to real-time 3D-applications of fUS in rodent models (Brunner et al., 2020; Edelman and Macé, 2021; Rabut et al., 2019). For a hemodynamics-based technique such as fUS to also reach its clinical and neuroscientific maturity, the fUS signal needs to be understood in relation to the underlying neuronal activity and its significance needs to be compared to other NVC-based functional techniques. In previous rodent work, Aydin et al. (Aydin et al., 2020) investigated '*the extent to which fUS faithfully reports local neuronal activation*' by combining fUS and two-photon microscopy (2PM) in a co-registered single voxel brain volume of a rodent model. The authors concluded that the transfer functions they could define, were robust across a wide range of stimulation paradigms and animals. Similarly,

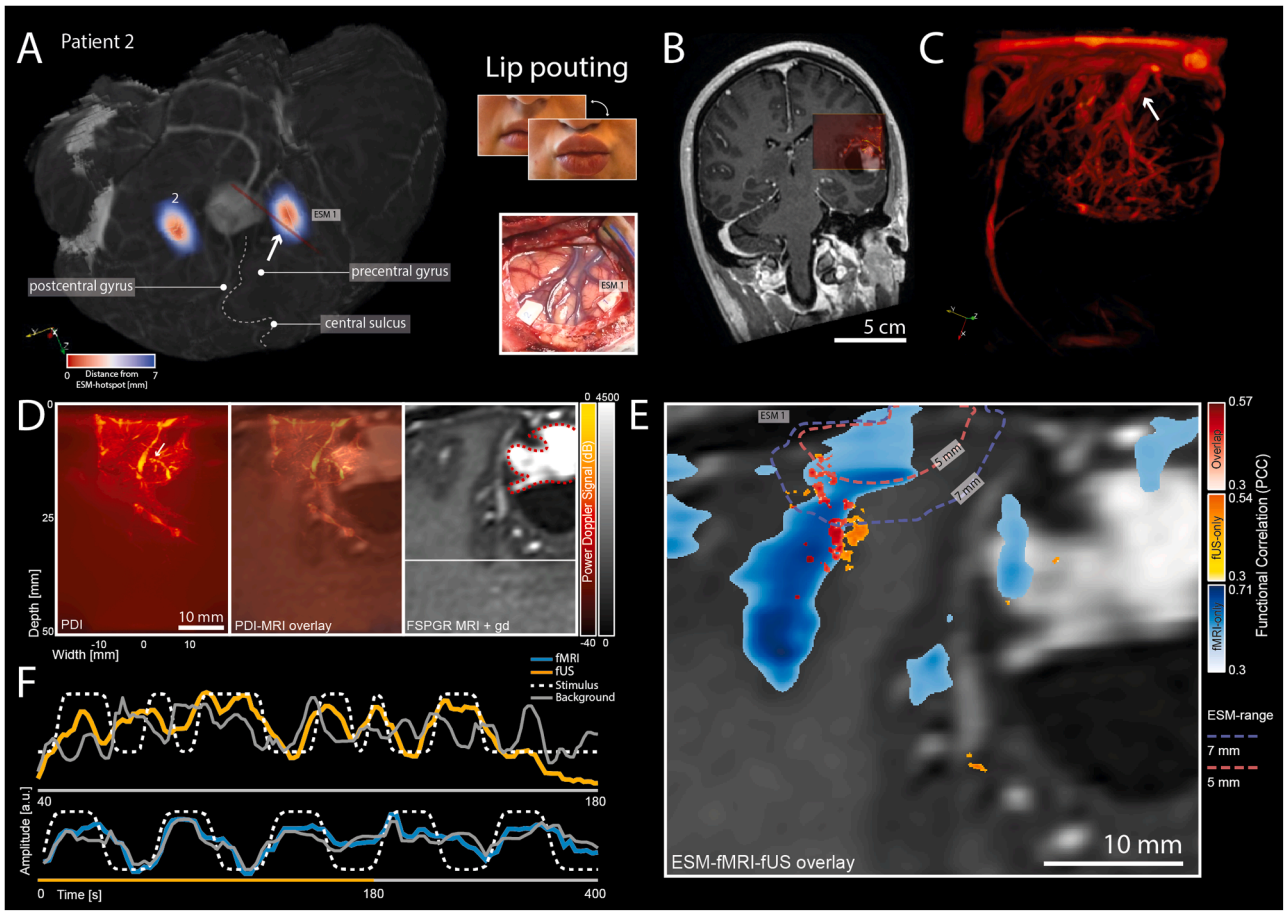

Fig. 4. Paired ESM-, fMRI- and fUS-acquisition in Patient 2: Motor Paradigm (lip pouting). A) Patient 2 underwent awake craniotomy surgery for the removal of an LGG in the left temporal lobe. The segmented 3D-reconstruction of the cerebrum is based on the pre-operative 3D-IR FSPGR T1-weighted MRI after administration of a gadolinium-based contrast agent. Intra-operative ESM was able to identify one stimulation site (*marker 1*) responsible for twitching of the mouth, confirming localization near the mouth motor cortex (*precentral gyrus*). The probe was placed over this area, with the orientation of the PDI during acquisition also depicted here relative to the 3D-MRI. **B)** Depiction of the co-registered MRI-slice corresponding to the 2D-ultrasound plane (*red*) described in (A). **C)** 3D- reconstruction of the tumor vasculature based on 2D-PDIs acquired intra-operatively. This volume exemplifies the level of microvascular detail which could be visualized intra-operatively using fUS. The tumor's vessels present with an arborous organization originating from what seems one main vessel (*white arrow)*. **D)** Side-by-side comparison of the structural 2D-PDI (*left panel)* and corresponding 2D-MR-image (*right panel*), as well as their overlay (*middle panel*). The 2D-image again depicts the arborous organization within the tumor (*white arrow)*. The white rectangle in the right panel depicts the ROI used for functional analysis. **E)** Thresholded (PCC>0.3) functional maps of the fUS-based (*yellow*), fMRI-based (*blue*) and fMRI-fUS overlapping (*red*) PCC-maps overlayed over the structural MRI. The the contours of the 7- and 5-mm zones of ESM-activation are depicted with the pink and purple dotted lines. We see clear overlap between the three techniques, although less clear as compared to the lip pouting task in Patient 1 (Fig. 3E). **F)** Overview of the functional signal in the fUS-defined functional areas (*yellow line*) and the fMRI-defined functional areas (*blue line*). The stimulus pattern (*white dotted line*) as used for the fUS-recording was significantly shorter and consisted of more randomized ON-durations as compared to the one used pre-operatively for fMRI. The average background signal of all the non-functional (PCC<0.3) pixels within the ROI is depicted in gray.

LGG = Low Grade Glioma, (f)MRI = (functional) Magnetic Resonance Imaging, fUS = functional Ultrasound, gd = gadolinium, ESM = Electrocortical Stimulation Mapping, ROI = Region of Interest, PCC = Pearson Correlation Coefficient, PDI = Power Doppler Image.

Nunez-Elizalde et al. (Nunez-Elizalde et al., 2022) performed simultaneous fUS and neural recordings during a visual paradigm in mice, and demonstrated how the fUS-signal seemed to '*accurately reflect neural activity both in time and in space*'. Along the same line, Boido et al. (Boido et al., 2019) report sequential imaging with 2PM-, fUS- and BOLD-fMRI-imaging of a mouse brain using an odor response-paradigm. Indeed, the authors concluded that '*fUS and BOLD-fMRI global signals showed the same linear relationship with locally measured neuronal* Ca^{2+}, (Boido et al., 2019), but the question is to what extent these relations hold in humans.

The introduction of fUS as a new imaging modality could shed new light on our understanding of NVC itself, a complex phenomenon which still remains to be fully elucidated to this day (Iadecola, 2017). By comparing and contrasting fUS-based functional maps to conventional modalities such as fMRI or ESM, we might be able to detangle different physiological contributions to these functional maps.

Conventionally, BOLD-fMRI is thought to indirectly probe neuronal activity through evoked cerebral blood volume (CBV), flow (CBF) and oxygenation changes (Logothetis et al., 2001; Uludağ and Blinder, 2018). However, the vascular dynamics determining the spatiotemporal characteristics of this BOLD-signal remain poorly understood on multiple levels. Structurally, much of our knowledge of human brain (micro) vasculature is based on in-human postmortem studies, in-human CT- or MR-angiography at millimeter-scale or through interpolation from animal studies, which are limited given the many species-dependent differences (Uludağ and Blinder, 2018). Functionally, we lack knowledge on vascular behavior such as CBV- and CBF-changes in different brain regions, under different baseline or stimulus-induced conditions (Uludağ and Blinder, 2018). fUS can capture both *in-vivo* hemodynamics as well as the underlying microvascular morphology, as we exemplified

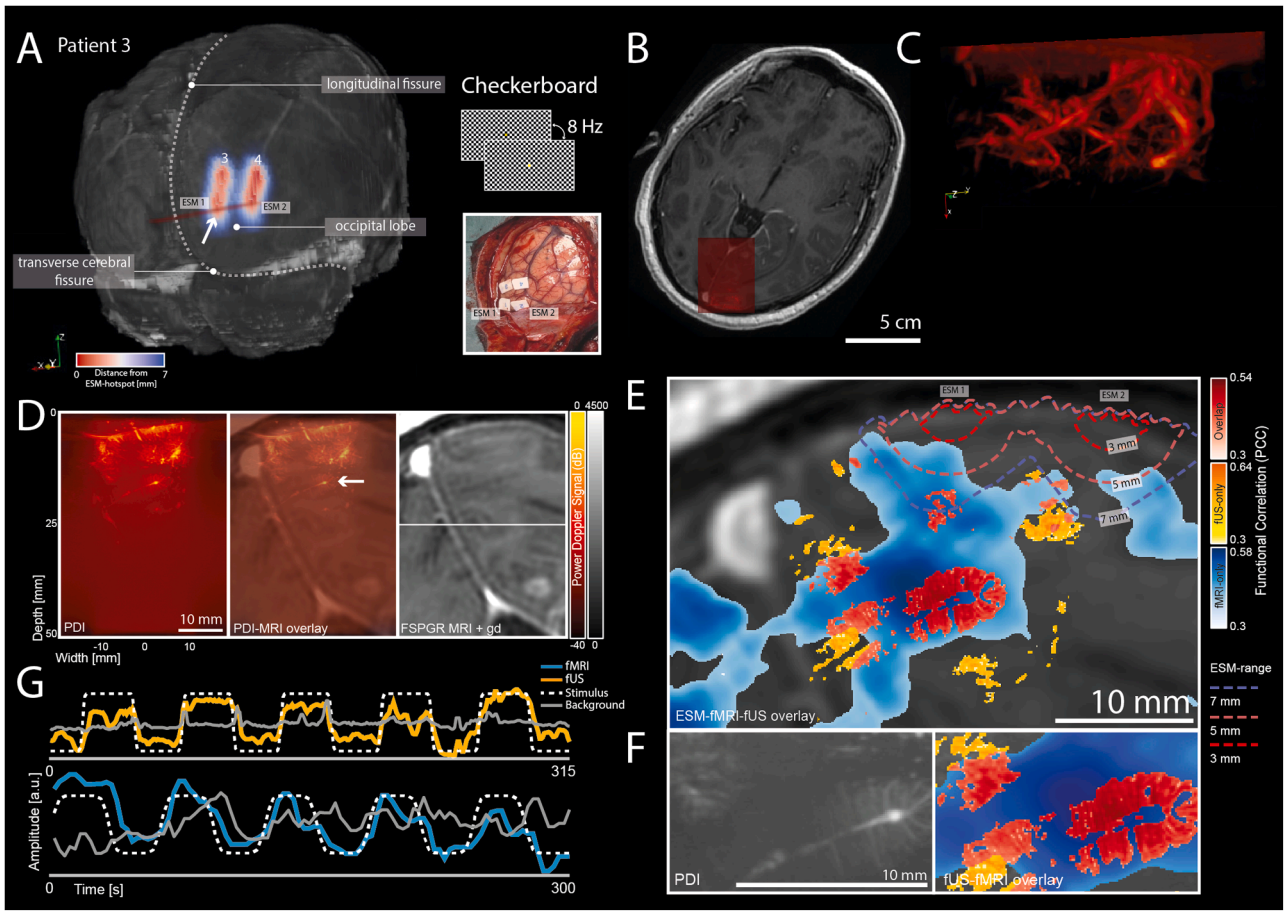

Fig. 5. Paired ESM-, fMRI- and fUS-acquisition in Patient 3: Visual Paradigm (8 Hz checkerboard). (**A**) Patient 3 underwent awake craniotomy surgery for the removal of an HGG in the right parietal lobe. The tumor is segmented in green here and visualized within the 3D-reconstruction of the facial contour, based on the pre-operative 3D-IR FSPGR T1-weighted MRI after administration of a gadolinium-based contrast agent. Intra-operative ESM was able to identify several stimulation sites responsible for reported visual light flashes (*marker 1–4*), confirming the localization of the visual cortex (*green asterisks*). The probe was positioned over these areas using the intra-operative arm, co-guided by the pre-operatively defined fMRI-ROIs based on an 8 Hz checkerboard visual task. The ultrasound plane is depicted in red here and positioned relative to the 3D-MRI. (**B**) Depiction of the co-registered MRI-slice corresponding to the 2D-ultrasound plane (*red*) described in (A). (**C**) 3D-vascular volume reconstructed from 2D-PDIs acquired intra-operatively during a sweeping motion over the craniotomy. (**D**) Side-by-side comparison of the structural 2D-PDI (*left panel)* and corresponding 2D-MR-image (*right panel*), as well as their overlay (*middle panel*). The overlay confirms the accuracy of the fUS-MRI co-registration. The PDI shows vascular details of healthy cortical vasculature, including a feather-like horizontal vessel at approximately 2 cm depth (*white arrow*). The white rectangle in the right panel depicts the ROI used for functional analysis. (**E**) Thresholded (PCC>0.3) functional maps of the fUS-based (*yellow*), fMRI-based (*blue*) and fMRI-fUS overlapping (*red*) PCC-maps overlayed over the structural MRI. We see clear overlap between the two techniques. (**F**) Zoom-in on the grayscale PDI of the feather-like vascular structure discussed in (D) (*left panel*). Zoom-in on the same region of the functional map also shown in (E) (*right panel*). The fUS-map seems to clearly follow the architecture of this vessel, whereas the fMRI-map seems to span a much larger region. (**G**) Overview of the functional signal in the fUS-defined functional areas (*yellow line*) and the fMRI-defined functional areas (*blue line*). In this case, the stimulus pattern (*white dotted line*) as used for the fUS- and fMRI-recording were similar and consisted of a 30 s ON- and OFF-period.

HGG = High Grade Glioma, (f)MRI = (functional) Magnetic Resonance Imaging, fUS = functional Ultrasound, FSPGR = fast spoiled gradient-echo, gd = gadolinium, ESM = Electrocortical Stimulation Mapping, ROI = Region of Interest, PCC = Pearson Correlation Coefficient, PDI = Power Doppler Image.

in e.g. Fig. 3D and Fig. 5D, E, opening up possibilities for concomitant *in-vivo* interrogation of vascular morphology and physiology. Using microbubble contrast, even higher resolution images of human brain microvasculature could be acquired through a technique called Ultrafast Localization Microscopy (ULM) (Errico et al., 2015), as was recently also demonstrated in humans (Demené et al., 2021). The fUS-signal itself is thought to reflect information on CBV, CBF, vascular tonus and flow directionality (Mace et al., 2013). fUS' ability to capture real-time hemodynamics and flow directionality, would allow for e.g. separated quantification of venous and arterial flow in the cortex based on flow directionality (Mace et al., 2013). In the context of CBV, the arterial contribution to CBV-increase is more significant and more localized as compared to the veins (Kim et al., 2007). Being able to study NVC-related signals with fUS could add a unique and valuable perspective to increase the field's general understanding of vascular phenomena.

Future work should focus on expanding not only the spatial but also the temporal characteristics of the fUS- and fMRI-signal in human brain tissue, for example in concomitance with neuronal signal recorded with ECoG-grids or neuronal activity evoked with bipolar stimulation. Here, it would also be interesting to further study the observed differences in the size of the functional maps found with fUS and fMRI: the fMRI-defined maps presented consistently with larger, non-overlapping functional areas (see e.g. Fig. 3E). This difference was consistent when studying fUS-fMRI-ESM overlap across different correlational thresholds (PCC>0.1, PCC>0.3 or PCC>0.5, see Supplementary Fig. 1), as well as different fMRI-analysis methodologies (Pearson's Correlation vs. Generalized Linear Model (GLM), see Supplementary Fig. 1). Potential explanations for these larger fMRI-defined maps remain to be elucidated, but could range from differences in spatial resolution between the

fMRI- and fUS-based maps, to less 'biological resolution' or spatial specificity of the BOLD-signal as compared to the Doppler-signal. A more quantitative analysis of the (non)-overlap between the functional maps could be insightful in better understanding the similarities and differences across the modalities. Given the proof-of-concept nature of our study, we have chosen for a primarily qualitative, descriptive approach, with a limited series of quantitative measures presented in our supplementary material. Follow-up studies with larger number of datasets, and perhaps even multiple repetitions of the same functional task, would leave more room for meaningful quantitative comparisons.

Using concomitant fUS with ESM could also improve our understanding of the mechanisms underlying this gold standard technique. Although ESM is thought to be the only technique which provides *direct* functional feedback on *necessary* brain regions involved in a functional task, literature also warns us to not be '*deluded by the obvious fascination of direct access to the human brain*' which ESM offers (Borchers et al., 2011).

Ultimately, we foresee a future for fUS as an intra-operative brain mapping technique in concomitance with - or perhaps at one point replacing - pre-operative fMRI. Using real-time, volumetric fUS brain imaging, the neurosurgeon could potentially see changes in functional brain activity as he is removing the tumor, opening up avenues for more continuous neuromonitoring as compared to point-based ESM. This is also large step forward compared to fMRI-based surgical decision-making, where one single pre-operative functional snapshot is used to guide intra-operative decision-making. Not only does intra-operative brain shift compromise the intra-operative accuracy of these fMRI-maps, there is also no real-time feedback on the functional consequences of the tumor removal. However, for fUS to see actual clinical maturity, several limitations still need to be addressed. First, we will need to move away from 2D-fUS to real-time 3D-fUS acquisitions. Not only will these volumetric measurements allow us to map more brain tissue at once, it will also aid in better tackling one of our main bottlenecks for actual successful functional mapping: motion artefacts. This problem is further exaggerated when performing 2D-imaging given the risk of out-of-plane motion. Second, we will need to find ways to facilitate high data-rate processing in the intraoperative setting, to be able to map and display volumetric functional brain activity in real-time in the operating room.

For now, the neurosurgical operating room will remain the primary context of application of clinical fUS: to this day, signal aberration as caused by the human skull still proves to be a challenge for fUS-based mapping of human brain activity.

5. Conclusions

This paper is the first in-human comparison between ESM-, fMRI- and fUS-imaging data. Using three different functional paradigms, we demonstrate consistent spatial overlap between the regions detected with the three techniques, with the added benefit of fUS being able to morphologically discern both the superficial and deep (>5 cm) vascular architecture underlying its hemodynamics-based functional maps. The current results rely heavily on a newly developed clinically integrated study pipeline allowing for co-registered multimodal brain mapping in the same human subject.

The work presented in this report serves as an important milestone towards clinical and neuroscientific maturity of fUS, and further showcases the synergistic potential this technique could have in increasing our understanding of hemodynamics-based functional imaging in general.

Credit author statement

SS and PK conceptualized the study with the help of DDS and MS. SS, EC, LV, DDS, EMB, JWS, BSF, FM and AJPEV were involved in data collection. SS, MS and PK performed the data-analysis. SS and PK wrote the first draft of the manuscript, with input from all authors. All authors provided input for and approved the final version of the manuscript.

Data availability

Raw data and source code will be shared upon reasonable request to the corresponding author.

Funding

This work was supported was supported by the NWO-Groot grant of The Dutch Organization for Scientific Research (NWO) (Grant no. 108845), awarded to CUBE (Center for Ultrasound and Brain-Imaging @ Erasmus MC, see for website: www.ultrasoundbrainimaging.com), as well as by the Netherlands Organization for Scientific Research (NWO-ALW 824.02.001; CIDZ), the Dutch Organization for Medical Sciences (ZonMW 91120067; CIDZ), Medical Neuro-Delta (MD 01092019–31082023; CIDZ), and INTENSE LSH—NWO (TTW/ 00798883; CIDZ).

Declaration of Competing Interest

The authors have no relevant competing interests to declare.

Acknowledgements

The authors would like to thank all members of the Erasmus MC neurosurgical OR- and MRI-team who significantly contributed to the realization of the project, including but not limited to Hanneke Muharam-Kamminga, Willem van 't Leven, Reinier van Elsäcker, Jolanda van den Berg, Josiane Wink-Godschalk, Markus Klimek and Ismail Eralp. The authors would like to especially thank Geert Springeling of the department of Experimental Medical Instrumentation (EMI), Erasmus MC, for his help in building the custom intra-operative surgical arm.

Supplementary materials

Supplementary material associated with this article can be found, in the online version, at doi:10.1016/j.neuroimage.2023.120435.

References

Aydin, A.K., Haselden, W.D., Goulam Houssen, Y., Pouzat, C., Rungta, R.L., Demené, C., Tanter, M., Drew, P.J., Charpak, S., Boido, D., 2020. Transfer functions linking neural calcium to single voxel functional Ultrasound signal. Nat. Commun. 11, 2954.

Baranger, J., Demene, C., Frerot, A., Faure, F., Delanoë, C., Serroune, H., Houdouin, A., Mairesse, J., Biran, V., Baud, O., Tanter, M., 2021. Bedside functional monitoring of the dynamic brain connectivity in human neonates. Nat. Commun. 12, 1080.

Boido, D., Rungta, R.L., Osmanski, B.F., Roche, M., Tsurugizawa, T., Le Bihan, D., Ciobanu, L., Charpak, S., 2019. Mesoscopic and microscopic imaging of sensory responses in the same animal. Nat. Commun. 10, 1110.

Borchers, S., Himmelbach, M., Logothetis, N., Karnath, H.O., 2011. Direct electrical stimulation of human cortex-the gold standard for mapping brain functions? Nat. Rev. Neurosci. 13, 63–70.

Brunner, C., Grillet, M., Sans-Dublanc, A., Farrow, K., Lambert, T., Macé, E., Montaldo, G., Urban, A., 2020. A platform for brain-wide volumetric functional Ultrasound imaging and analysis of circuit dynamics in awake mice. Neuron 108, 861-875.e7.

Deffieux, T., Demene, C., Pernot, M., Tanter, M., 2018. Functional Ultrasound neuroimaging: a review of the preclinical and clinical state of the art. Curr. Opin. Neurobiol. 50, 128–135.

Demene, C., Baranger, J., Bernal, M., Delanoe, C., Auvin, S., Biran, V., Alison, M., Mairesse, J., Harribaud, E., Pernot, M., Tanter, M., Baud, O., 2017. Functional Ultrasound imaging of brain activity in human newborns. Sci. Transl. Med. 9, eaah6756.

Demené, C., Robin, J., Dizeux, A., Heiles, B., Pernot, M., Tanter, M., Perren, F., 2021. Transcranial ultrafast ultrasound localization microscopy of brain vasculature in patients. Nat. Biomed. Eng. 5, 219–228.

Dizeux, A., Gesnik, M., Ahnine, H., Blaize, K., Arcizet, F., Picaud, S., Sahel, J.A., Deffieux, T., Pouget, P., Tanter, M., 2019. Functional Ultrasound imaging of the brain reveals propagation of task-related brain activity in behaving primates. Nat. Commun. 10, 1400.

Edelman, B.J., Macé, E., 2021. Functional Ultrasound brain imaging: bridging networks, neurons, and behavior. Curr. Opin. Biomed. Eng. 18.
Errico, C., Osmanski, B.F., Pezet, S., Couture, O., Lenkei, Z., Tanter, M., 2016. Transcranial functional Ultrasound imaging of the brain using microbubble-enhanced ultrasensitive Doppler. Neuroimage 124, 752–761.
Errico, C., Pierre, J., Pezet, S., Desailly, Y., Lenkei, Z., Couture, O., Tanter, M., 2015. Ultrafast ultrasound localization microscopy for deep super-resolution vascular imaging. Nature 527, 499–502.
Fedorov, A., Beichel, R., Kalpathy-Cramer, J., Finet, J., Fillion-Robin, J.C., Pujol, S., Bauer, C., Jennings, D., Fennessy, F., Sonka, M., Buatti, J., Aylward, S., Miller, J.V., Pieper, S., Kikinis, R., 2012. 3D slicer as an image computing platform for the quantitative imaging network. Magn. Reson. Imaging 30, 1323–1341.
Gesnik, M., Blaize, K., Deffieux, T., Gennisson, J.L., Sahel, J.A., Fink, M., Picaud, S., Tanter, M., 2017. 3D functional Ultrasound imaging of the cerebral visual system in rodents. Neuroimage 149, 267–274.
Hacker, C.D., Roland, J.L., Kim, A.H., Shimony, J.S., Leuthardt, E.C., 2019. Resting-state network mapping in neurosurgical practice: a review. Neurosurg. Focus 47, E15.
Iadecola, C., 2017. The neurovascular unit coming of age: a journey through neurovascular coupling in health and disease. Neuron 96, 17–42.
Imbault, M., Chauvet, D., Gennisson, J.L., Capelle, L., Tanter, M., 2017. Intraoperative functional Ultrasound imaging of human brain activity. Sci. Rep. 7, 7304.
Kim, T., Hendrich, K.S., Masamoto, K., Kim, S.G., 2007. Arterial versus total blood volume changes during neural activity-induced cerebral blood flow change: implication for BOLD fMRI. J. Cereb. Blood Flow Metab. 27, 1235–1247.
Logothetis, N.K., Pauls, J., Augath, M., Trinath, T., Oeltermann, A., 2001. Neurophysiological investigation of the basis of the fMRI signal. Nature 412, 150–157.
Macé, E., Montaldo, G., Cohen, I., Baulac, M., Fink, M., Tanter, M., 2011. Functional Ultrasound imaging of the brain. Nat. Methods 8, 662–664.
Mace, E., Montaldo, G., Osmanski, B.F., Cohen, I., Fink, M., Tanter, M., 2013. Functional Ultrasound imaging of the brain: theory and basic principles. IEEE Trans. Ultrason. Ferroelectr. Freq. Control 60, 492–506.
Martin, C., 2014. Contributions and complexities from the use of *in-vivo* animal models to improve understanding of human neuroimaging signals. Front. Neurosci. 8, 211.
Nathan, S.S., Sinha, S.R., Gordon, B., Lesser, R.P., Thakor, N.V., 1993. Determination of current density distributions generated by electrical stimulation of the human cerebral cortex. Electroencephalogr. Clin. Neurophysiol. 86, 183–192.
Norman, S.L., Maresca, D., Christopoulos, V.N., Griggs, W.S., Demene, C., Tanter, M., Shapiro, M.G., Andersen, R.A., 2021. Single-trial decoding of movement intentions using functional Ultrasound neuroimaging. Neuron 109, 554-1566.e4.
Nunez-Elizalde, A.O., Krumin, M., Reddy, C.B., Montaldo, G., Urban, A., Harris, K.D., Carandini, M., 2022. Neural correlates of blood flow measured by ultrasound. Neuron 110, 1631-1640.e4.
Osmanski, B.F., Pezet, S., Ricobaraza, A., Lenkei, Z., Tanter, M., 2014. Functional Ultrasound imaging of intrinsic connectivity in the living rat brain with high spatiotemporal resolution. Nat. Commun. 5, 7614.
Poldrack, R.A., Mumford, J.A., Nichols, T.E., 2011. Handbook of Functional MRI Data Analysis. Cambridge University Press.
Rabut, C., Correia, M., Finel, V., Pezet, S., Pernot, M., Deffieux, T., Tanter, M., 2019. 4D functional Ultrasound imaging of whole-brain activity in rodents. Nat. Methods 16, 994–997.
Rau, R., Kruizinga, P., Mastik, F., Belau, M., de Jong, N., Bosch, J.G., Scheffer, W., Maret, G., 2018. 3D functional Ultrasound imaging of pigeons. Neuroimage 183, 469–477.
Ritaccio, A.L., Brunner, P., Schalk, G., 2018. Electrical stimulation mapping of the brain: basic principles and emerging alternatives. J. Clin. Neurophysiol. 35, 86–97.
Soloukey, S., Vincent, A.J.P.E., Satoer, D.D., Mastik, F., Smits, M., Dirven, C.M.F., Strydis, C., Bosch, J.G., van der Steen, A.F.W., De Zeeuw, C.I., Koekkoek, S.K.E., Kruizinga, P., 2020. Functional Ultrasound (fUS) during awake brain surgery: the clinical potential of intra-operative functional and vascular brain mapping. Front. Neurosci. 13, 1384.
Stopa, B.M., Senders, J.T., Broekman, M.L.D., Vangel, M., Golby, A.J., 2020. Preoperative functional MRI use in neurooncology patients: a clinician survey. Neurosurg. Focus 48.
Tokuda, J., Fischer, G.S., Papademetris, X., Yaniv, Z., Ibanez, L., Cheng, P., Liu, H., Blevins, J., Arata, J., Golby, A.J., Kapur, T., Pieper, S., Burdette, E.C., Fichtinger, G., Tempany, C.M., Hata, N., 2009. OpenIGTLink: an open network protocol for image-guided therapy environment. Int. J. Med. Robot. Comput. Assist. Surg. 5, 423–434.
Uludağ, K., Blinder, P., 2018. Linking brain vascular physiology to hemodynamic response in ultra-high field MRI. Neuroimage 168.
Urban, A., Dussaux, C., Martel, G., Brunner, C., Mace, E., Montaldo, G., 2015. Real-time imaging of brain activity in freely moving rats using functional Ultrasound. Nat. Methods 12, 873–878.
Vlieger, E.J., Majoie, C.B., Leenstra, S., den Heeten, G.J., 2004. Functional magnetic renosance imaging for neurosurgical planning neurooncology. Eur. Radiol. 14, 1143–1153.